Density Functional Calculations of ATP Systems. 2. ATP Hydrolysis at the Active Site of Actin

J. Akola[†] and R. O. Jones*

Institut für Festkörperforschung, Forschungszentrum Jülich, D-52425 Jülich, Germany

Received: August 31, 2005; In Final Form: February 8, 2006

The hydrolysis of adenosine 5′-triphosphate (ATP) at the active site of actin has been studied using density functional calculations. The active site is modeled by the triphosphate tail of ATP, an Mg cation, surrounding water molecules, and the nearby protein residues. Four reaction paths have been followed by constraining coordinates that allow phosphate stretching, nucleophilic attack of the catalytic water, and OH^- formation via water deprotonation. The lowest-energy barrier (21.0 kcal/mol) is obtained for a dissociative reaction where the terminal phosphate breaks on approaching the catalytic water, followed by proton release via a proton wire mechanism. A higher barrier (39.6 kcal/mol) results for an associative reaction path where OH^- is formed first, with a pentacoordinated phosphorus atom (P−O distances 2.1 Å). Stretching the terminal bridging P−O bond results in bond rupture at 2.8 Å with an energy barrier of 28.8 kcal/mol. The residues Gln137 and His161 are not important in the reactions, but insight into their roles in vivo has been obtained. The favored coordination of the end products $H_2PO_4^-$ and ADP^{3-} includes a hydrogen bond and an O−Mg−O bridge between the phosphates as well as a hydrogen bond between $H_2PO_4^-$ and the Ser14 side chain. The total energy is 2.1 kcal/mol lower than in the initial reactants. Classical simulations of ATP− and ADP·P_i−actin show few hydrolysis-induced differences in the protein structure, indicating that phosphate migration is necessary for a change in conformation.

I. Introduction

Adenosine 5′-triphosphate (ATP), the universal energy carrier in the living cell, consists of adenosine linked to three phosphate groups. Removal of the outermost γ-phosphate to form adenosine diphosphate (ADP) provides energy for use in other reactions. With provision of energy, the inorganic phosphate group P_i can be bound to ADP to form ATP. The formation and use of ATP is "the most prevalent chemical reaction in the human body" and "the principal net chemical reaction occurring in the whole world".[1] It is not surprising that it has been studied in a vast array of contexts, and we focus here on the mechanism of this reaction at the active site in the protein actin.

Actin (molecular weight 43 kDa) comprises two domains connected by an α-helix, and the overall shape resembles a cloverleaf with a deep interdomain cleft that can bind one adenine nucleotide (ADP or ATP) complexed with a divalent cation (Mg^{2+} or Ca^{2+}). ADP/ATP is essential for the stability of actin under physiological conditions.[2] Actin is involved in muscle contraction, cellular motility and division (cytokinesis), vesicle transport, and the establishment and maintenance of cell morphology. It is also an essential component of structures such as the intestinal brush border or the sensory cells of the inner ear (stereocilia). The versatility of actin is a consequence of the dynamic nature of filamentous actin (F-actin) assemblies that form in living organisms. In the cytoplasm of a cell, a microscopic network of actin filaments (cytoskeleton) is formed via polymerization of actin monomers (G-actin). The contribution of the ATP/ADP reaction to the structure, function, and dynamics of actin is crucial in this context, and most actin subunits hydrolyze a single molecule of ATP to ADP during the lifetime of F-actin. Hydrolysis involves cleavage of the terminal bridging P−O bond between β- and γ-phosphates (rate 0.035 s^{-1} at 20 °C),[3] followed by slow liberation of the resulting inorganic phosphate from the protein (0.0026 s^{-1}).[3]

In an earlier study, we performed density functional (DF) calculations of the hydrolysis of ATP to yield ADP and P_i in an aqueous environment,[4] and we extend this work here to ATP hydrolysis at the active site of actin. Density functional calculations incorporate details of the electronic structure of ATP, water molecules, and the active site without introducing adjustable parameters, and our goal is to provide an atomistic description of plausible reaction paths. The protein plays a crucial role, since it affects the properties of ATP and deprotonation affinity (pK_a) of the reactive water molecule. Furthermore, the coordination of the end products can aid understanding of the energetics, the possible conformational changes due to hydrolysis, and the phosphate migration that completes the process.

The structures studied here are based on the X-ray measurement of *Saccharomyces cerevisiae* (yeast) actin bound to gelsolin segment-1,[5] one of the few measurements that includes the Mg^{2+}−ATP metal nucleotide at the center of G-actin. Although the hydrolysis of G-actin is slow, it is over 3 orders of magnitude faster than that for the solvent-catalyzed reaction,[6] and hydrolysis-inhibiting factors (gelsolin) must be used. The corresponding structure does not provide an environment where ATP hydrolysis occurs spontaneously, but it enables DF calculations and experiment to be compared. The second step of ATP hydrolysis in actin involves a reorientation and subsequent migration of the cleaved phosphate, and classical

* Author to whom correspondence should be addressed. E-mail: r.jones@fz-juelich.de.

[†] Present address: Nanoscience Center, Department of Physics, University of Jyväskylä, P.O. Box 35, Jyväskylä FI-40014, Finland.

10.1021/jp054921d CCC: $30.25
Published on Web 03/25/2006

molecular mechanics simulations provide additional information. In section II we outline the methods of calculation that we have used, and the results are presented in section III. Our concluding remarks are given in section IV.

II. Methods of Calculation

The Car−Parrinello molecular dynamics (CPMD) package[7] is based on DF theory and was used for most of the calculations in the companion paper.[8] The approximation of Perdew, Burke, and Ernzerhof (PBE) is used for the exchange−correlation energy,[9] and the plane wave basis set has a kinetic energy cutoff of 80 Ry. The electron−ion interaction is described by nonlocal, norm-conserving, and separable pseudopotentials;[10] for the metal cations Na^+, Mg^{2+}, and Ca^{2+}, the contribution of semicore electrons is included as discussed in ref 8. The interaction between (charged) replicas is avoided by solving the Poisson equation using the method of Hockney.[11] Geometries are optimized using the simulated annealing procedure, where the backbone atoms (N, C_α, C) and the side chain terminating aliphatic carbons are fixed to preserve the original actin conformation.

The initial protein coordinates were taken from the X-ray measurement of globular yeast actin (G-actin) bound to a gelsolin segment (PDB code 1YAG) with a metastable Mg^{2+}−ATP complex inside.[5] Our earlier work on ATP hydrolysis in water[4] showed that ATP can be approximated by methyl triphosphate (MTP), and the present reactions are based on MTP^{4-} complexed with Mg^{2+}. The active site of actin is modeled by selecting MTP,[4−] Mg^{2+}, the likely catalytic water (WAT709),[5] and the actin residues and water oxygens within 5 Å. This model contains 18 residues and 10 water molecules, where missing hydrogens have been added using simple chemical rules. The water molecules are placed to saturate the hydrogen bond (H-bond) network, and some residue side chains (residues Asp11, Lys18, Gln137, Asp154, and His161) are terminated by hydrogen atoms to compensate for missing backbone links. For the residues interacting via backbone atoms with the functional parts (MTP^{4-}, Mg^{2+}, and reactive H_2O), termination occurs at the α-carbon (C_α) belonging to the first residue outside the cutoff radius. This avoids cutting peptide bonds. The side chains pointing away from the system center are terminated at the next aliphatic carbon (C_β).

The active site of actin then comprises 222 atoms (652 valence electrons) and is shown from two perspectives in Figure 1. Positively (Mg^{2+}, Lys18) and negatively charged (MTP,[4−] Asp11, Asp154) groups are present, and the total charge is −3. His161 is chosen to be deprotonated at N_δ, since a short test calculation indicated that the protonated form is unstable in this context. The triphosphate is clamped between three β-hairpin loops (P-loops), labeled as P1, P2, and P3, where the homologous P1 (residues Gly13, Ser14, Gly15, and Met16) and P2 loops (Gly156, Asp157, Gly158, and Val159) make several H-bonds with MTP, whereas P3 (Gly302) has only one linkage to the α-phosphate. Residues His73 (side chain terminated) and Gly74, which do not interact with the triphosphate directly, form a sensor loop that has been proposed to intermediate conformational changes upon P_i release.[12,13] The reactive part near the terminal phosphate includes four water molecules (WAT1−WAT4) and is confined from the other side by the sensor loop, the side chains of His161 and Val159, and the backbone segment consisting of Ala108 and Pro109. The terminated side chains of Asp11 and Asp154 stabilize the Mg^{2+} hydration shell, and the lysine finger (Lys18) points toward the β-phosphate. The Gln137 side chain is connected with the catalytic WAT1, which is ideally positioned for a nucleophilic attack.[5]

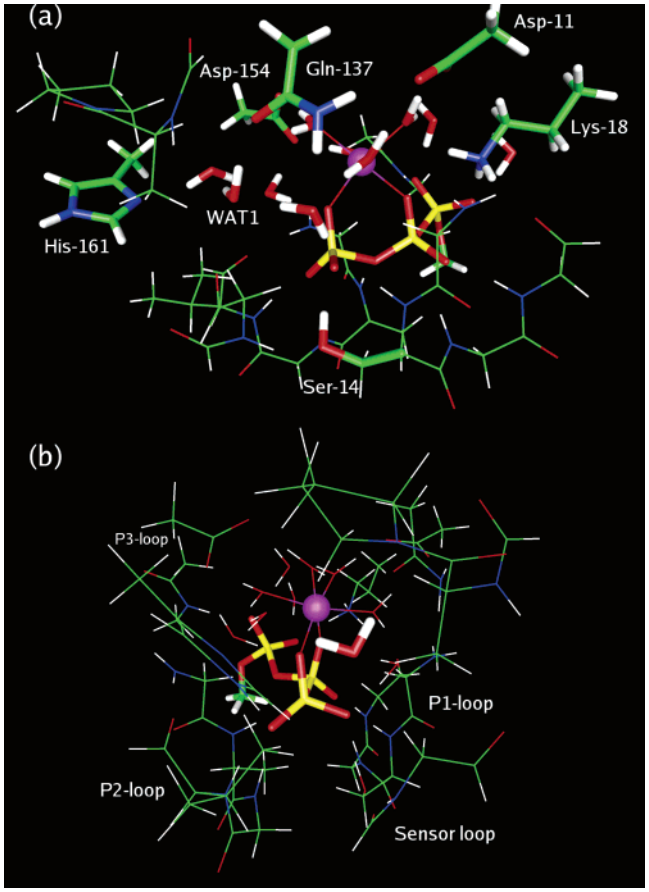

Figure 1. Simulated active site of actin shown from two perspectives. (a) Front view: The triphosphate tail of ATP, water molecules, and residue side chains are plotted in licorice representation, and the Mg cation is the magenta sphere. (b) Side view: The triphosphate and catalytic water are emphasized (notice the location of WAT1), and the protein β-hairpin segments are labeled. Color key: hydrogen, white; carbon, green; nitrogen, blue; oxygen, red; phosphorus, yellow.

The reactions are modeled by constraining three reaction coordinates and optimizing the remaining degrees of freedom, and the first one studied was the distance between the terminal phosphorus P_γ and the bridging anhydride oxygen O_s

$$d(\mathbf{r}_{P_\gamma}, \mathbf{r}_{O_s}) = |\mathbf{r}_{P_\gamma} - \mathbf{r}_{O_s}| \tag{1}$$

which describes the P_γ−O_s bond breaking. A modification of the first incorporates the difference between two distances

$$d(\mathbf{r}_{P_\beta}, \mathbf{r}_{P_\gamma}, \mathbf{r}_{O_w}) = |\mathbf{r}_{P_\gamma} - \mathbf{r}_{P_\beta}| - |\mathbf{r}_{P_\gamma} - \mathbf{r}_{O_w}| \tag{2}$$

where O_w stands for the oxygen atom of WAT1. This constraint forces the catalytic water to approach the terminal phosphorus while the two phosphates separate. The third is the proton coordination number of WAT1

$$n_H(\mathbf{r}^{N_H}, \mathbf{r}_{O_w}) = \sum_{i=1}^{N_H} S(|\mathbf{r}_{H_i} - \mathbf{r}_{O_w}|) \tag{3}$$

where $\mathbf{r}^{N_H}$ denotes the set of the positions of the H atoms and

$$S(r) = \frac{1}{\exp[\kappa(r - r_c)] + 1} \tag{4}$$

is the Fermi distribution with a cutoff radius and width of r_c = 1.38 Å, κ^{-1} = 0.1 Å, respectively.[14] A water molecule can be

converted into a hydroxyl ion by decreasing n_H from 2 to 1 (deprotonation). The conversion to a hydronium ion (from 2 to 3) has not been pursued here.

Reaction mechanisms are determined by changes in the free energy rather than total energy, and we calculated both for the smaller systems studied previously.[4] For the best equilibrated systems the changes in these two quantities were very similar, and measurements of a range of reactions related to ATP hydrolysis[15] showed that the effect of entropy (1−4 kcal/mol) is much smaller than the energy changes that we find here. This is very encouraging, because calculations of free energy differences in a system of this size would be immensely time-consuming. We note that the combination of DF calculation with a force field description of the surroundings (QM/MM) provides an attractive alternative to the "cluster" approach that we use.[16]

Information about the hydrolysis-induced changes in the actin environment has been found by performing 8−10 ns of classical molecular mechanics for the ATP−actin (situation before hydrolysis), ADP·P_i−actin (after hydrolysis), and ADP−actin (after phosphate migration) separately. The systems are embedded in an orthorhombic box of water (altogether 38 700 atoms) at 300 K with periodic boundary conditions. We used the ORAC simulation package,[17] which employs a multiscale time step, the smooth particle mesh Ewald (SPME) method for the electrostatic interaction,[18] and the AMBER99 force field for biomolecules.[19] For ATP and ADP, a recently developed force field with classical point charges is used,[20] and the Lennard-Jones parameters of Mg^{2+} (as well as those of Na^+ and Ca^{2+} counterions) are fitted to the DF calculations of hexahydrate in our companion article.[8] The solvent molecules are modeled with a TIP3 force field, and the missing phosphate in an ADP−actin starting structure is replaced with one H_2O. The covalent bonds involving H atoms are kept rigid with a matrix inversion method, and the multiple time step ranges from 0.333 fs (bond stretching) to 8 fs (long-range Coulomb and Lennard-Jones). Each simulation is preceded by an equilibration phase of 0.5 ns where the system is initialized both at constant temperature (300 K) and pressure (1 atm), and the data recording is performed in an NVT ensemble with three Nosé thermostats that are coupled to the solute, solvent, and center of mass separately.

III. Results

A. Optimized Active Site: Reactants. ATP resides in a cleft between two actin domains, where its triphosphate tail is captured between three P-loops forming hydrogen bonds with the backbone amide groups (Figure 1). The Mg^{2+} ion lies between the β- and γ-phosphates and forms a bidentate chelate configuration, and it has a typical hexacoordinated hydration shell with four water molecules stabilized by the two carboxylate groups (Asp11 and Asp154). The side chains in direct contact with ATP are Lys18 (binds to α- and β-phosphoryl oxygens) and Ser14 (terminal phosphate). The positively charged Lys18 is far from the water molecules surrounding the terminal phosphate. This does not favor catalytic activity, but its charge and that of Mg^{2+} balance the negative charge of MTP^{4-}. It is also coupled directly to a Mg^{2+}-coordinating H_2O and β-phosphoryl oxygen, so that the bidentate chelate configuration can be modified. Ser14 and its link with ATP play crucial roles in actin conformation; in the presence of ADP this side chain either connects with the β-phosphate (nonbridging oxygen) or flips to another rotamer, and it affects the nearby sensor loop (His73) in both cases. There is then a correlation between the bound nucleotide (ADP or ATP), the orientation of the Ser14 side chain, and the conformation of the sensor loop. Site-directed mutagenesis studies of residues Ser14,[21] His73,[13] Asp157,[21] Val159,[22] and Arg177[23] have shown that the residues in the vicinity of the nucleotide binding site are crucial for maintaining the interdomain geometry, but implications of a direct involvement in ATP hydrolysis are found only for residues Gln137 and His161 on the basis of X-ray measurements and genetic studies (viability in yeast).[5]

The terminal phosphate and four water molecules (WAT1−WAT4) form a loop of H-bonds. WAT1 is referred to as "catalytic", because its position allows a nucleophilic attack on the terminal phosphorus. We have optimized two structures where the orientation of this molecule is modified to form a hydrogen bond with the Gln137 side chain or the terminal phosphate. The resulting intermolecular $P_\gamma-O_w$ distances are 4.33 and 3.61 Å, respectively, the experimental value being 3.81 Å (or 4.01 Å for another type of actin with Mg^{2+}−ATP, see below).[5] The small variations in the $O_s-P_\gamma-O_w$ angles (all ∼160°) imply that the direction of H_2O changes little during optimization. For both structures, dipole moments of individual water molecules were calculated using localized Wannier orbitals,[24] and the results for WAT1 (3.1 and 2.7 D, respectively, with a total range of 2.7−3.5 D) are close to the average value of 3.0 D calculated for bulk water.[25] The energetic difference between the two optimized configurations is only 0.8 kcal/mol, and we have chosen the structure where WAT1 contacts Gln137 (Figure 1) as our starting point. This choice does not affect the path with the lowest-energy barrier because WAT1 rotates from the first orientation to the second as the reaction proceeds.

The His161 residue is assigned as the catalytic base in the nucleotide binding cavity,[5] because it is close to the likely water nucleophile, and other functional groups have unsuitable locations. His161 does not bind directly to WAT1 in the initial crystal structure, but it forms a hydrogen bond with a neighboring WAT2 ($N_\delta-O$ distance 2.66 Å). Structural optimization has little effect on the His161 orientation, and the H-bond remains at 2.91 Å ($N_\delta-H$ distance 1.96 Å, H-bond angle 159°). In addition to *S. cerevisiae*, Vorobiev et al.[5] have reported crystal structures of *Dictyostelium* actin with Ca^{2+}−ATP, Mg^{2+}−ATP, and Li^+−ATP. They noted that His161 occupies a similar position with divalent cations, whereas with Li^+−ATP the catalytic H_2O is directly coordinated by His161, indicating a high mobility of this side chain.

Structural properties of the triphosphate tail in different environments are given in Table 1. The calculated values for nonbridging P−O bonds are similar in aqueous solution, crystal, and ATP−actin, but they are longer than the experimental result for ATP−actin. Hydrogen bonding with water molecules is common to all environments as well as the interaction with a chelating cation. The terminal bridging $P_\gamma-O_s$ bond (O_s denotes anhydride oxygen) is slightly longer (1.72 Å) than those in other calculations. A possible cause is a direct H-bond between the anhydride oxygen and the amine group of Asp157, and such H-bonds are generally absent in water under normal conditions (T = 310 K, pH 7).[4] This anhydride bond is extended more than 0.1 Å from its experimental value, while the facing $P_\beta-O_s$ bond length is 1.61 Å. The Mg−O distances show larger deviations in the experiment, and this may arise because parts of the protein are not considered. The estimated effective charge of the cation is 1.2 electrons.[26]

Table 1 shows that typical values for the $P-O_s-P$ bridge angle are ∼130°. These values do not depend significantly on the attached cation, and the only exception in the case of free ATP is caused by the intramolecular hydrogen bonding (lack

TABLE 1: Structural Parameters of the ATP Triphosphate Tail in Different Environments[a]

	ATP (free)[b]	ATP (aq)[b]	ATP crystal[c]	ATP−actin (DF)	ATP−actin (expt)
P═O	1.50	1.50−1.55	1.50−1.54	1.51−1.55	1.44−1.52
P−O	1.57	1.50−1.55	1.59	1.51−1.55	1.44−1.52
P−O_s	1.58, 1.65	1.62−1.70	1.62−1.69	1.61−1.72	1.57−1.61
C−O_s	1.48	1.46	1.45	1.44	1.44
Mg−O		2.15		2.07−2.13	2.08−2.29
P−O_s−C	120	119	116/124	121	128
P−O_s−P	120	128	129−137	124, 131	133, 136
O_s−P_γ−O	105−109	104	101−110	101−106	105−109
O−Mg−O		90, 171		80−99, 167−179	82−103, 166−174
ω1	−100		68/−67	−39	−66
ω_1'	−151		71/176	161	156
ω2	−67		−63/142	158	155
ω_2'	−61		101/−53	−24	−28
Proj1	8		14/−42	−39	−52
Prof2	15		−32/31	20	28

[a] Apart from the experimental results in the last column, the values are calculated with a DF method. Torsional angles are calculated around bridging O1−P1 (ω_1), P1−O4 (ω_1'), O4−P2 (ω_2), and P2−O7 (ω_2') bonds. Projection angles Proj1 and Proj2 correspond to O−P···P−O configurations of α- and β-phosphates and β- and γ-phosphates, respectively. [b] From ref 4, the free molecule is neutral (triphosphate tail protonated), and there are no metal cations. [c] From ref 8, the $Na_2ATP{\cdot}3H_2O$ crystal consists of two types of ATP monomers (A/B).

of solvent). Furthermore, the O_s−P_γ−O angles are systematically lower than the tetrahedral value (109.47°) often used for phosphates in crystallography (the average difference is 6° for ATP−actin). These observations agree with a DF study of ATP in the active site of myosin.[27]

In the optimized active site,[28] the triphosphate acquires a relatively extended conformation with the three P atoms 2.9−3.0 Å apart (the angle P_α−P_β−P_γ is 130°). This differs from the ATP crystal salt,[8] where the triphosphate tails fold helically, and the angles are between 90 and 100°. The phosphate dihedral angles resemble the corresponding values of monomer B in the ATP crystal,[8] with some deviations in ω_1 (around the O_s−P_α bond) and ω_2' (around the P_β−O_s bond). The terminal methyl group is free to rotate during optimization (only the C atom is fixed), which causes a difference of 27° in ω_1. The phosphate projection angles (Proj1 and Proj2) show that conformations are generally neither staggered (±60°) nor eclipsed (0°).

The vibrational properties of the triphosphate tail, the complexed Mg cation, and four Mg-coordinating water molecules are calculated using a finite differences method with the rest of the system fixed. The highest-frequency modes between 2830 and 3780 cm^{-1} involve the O−H stretching of water molecules, and their wide range reflects differences in hydrogen bonding (aspartate side chains, water molecules). The H−O−H bending modes are blue-shifted to 1700−1780 cm^{-1}, and the P−O stretching modes lie between 1060 and 1220 cm^{-1}, followed by the radial breathing modes of the individual phosphate groups at 971 cm^{-1}. P−O_s stretching is distributed over two modes at 860 and 924 cm^{-1}, with the latter dominant. The P−O and P−O_s stretching frequencies agree well with the experimental values (1235 and 895 cm^{-1}) measured for ternary complexes of ATP, bis(2-pyridyl)amine, and divalent cations (infrared spectra).[29] The Mg−O stretching modes lie between 350 and 380 cm^{-1}.

B. Dissociative Reaction. The energetics of the first "dissociative" reaction are shown in Figure 2 together with the applied force of constraint and the P_γ−O_w and P_γ−P_β distances. This path involves stretching the terminal bridging P_γ−O_s bond and provides direct information about the covalent bond strength and the related restoring force. Shortening this bond to 1.57 Å results in an energy increase of 5.3 kcal/mol, implying that there is a significant energy difference between the theoretical result and the experimental bond length. Elongation to 2.00 Å costs a similar amount of energy, indicating an asymmetric potential

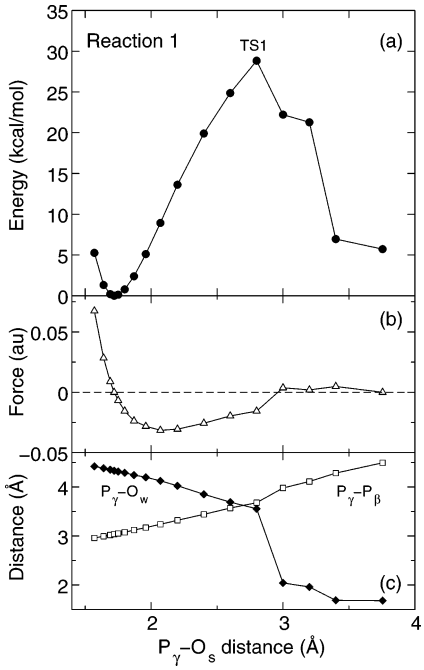

Figure 2. Dissociative reaction: (a) energetics, (b) force of constraint, and (c) P_γ−O_w and P_γ−P_β distances as a function of reaction coordinate P_γ−O_s.

energy curve. The magnitude of the restoring force increases gradually until 2.07 Å, after which it decreases slowly as the energy maximum is reached (28.8 kcal/mol at 2.8 Å). This phase involves a gradual formation of the planar PO_3^- unit, which interacts with a lone pair orbital of WAT1. After the energy maximum (anhydride bond breaking), the water nucleophile abruptly attacks the metaphosphate and forms an intermediate with a P_γ−O_w distance of 1.96 Å, where deprotonation has not yet occurred (P_γ−O_s distance 3.2 Å). A further increase of the separation of phosphate from ADP causes a proton transfer at 3.4 Å via a Grotthuss diffusion mechanism through two water molecules (WAT2 and WAT3) to a nonbridging O_γ. Finally, release of the constraint results in separated $H_2PO_4^-$ and ADP^{3-}, which are coupled by Mg^{2+}, and the corresponding total energy is 5.7 kcal/mol above the initial value.

The protein environment does not participate directly in the reaction, but there are changes in the terminal phosphate coordination. The gradual elongation of the P_γ−O_s bond breaks

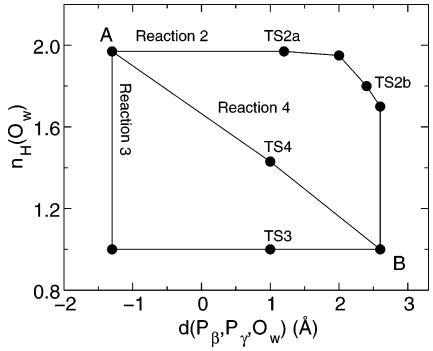

Figure 3. Reaction scheme for the reactions using two constraints: the protonation number of nucleophilic water $n_H(O_w)$ and the linear combination (difference) of distances $P_\gamma-P_\beta$ and $P_\gamma-O_w$ ($d(P_\beta,P_\gamma,O_w)$). The points A and B correspond to reactants and end product, respectively, and the transitions states are labeled according to the abbreviations used in the text.

three H-bond contacts between the nonbridging phosphoryl oxygens and the backbone amine groups of Ser14, Gly158, and Val159. The separated phosphate eventually makes contact with the Ser14 and Gln137 side chains (H-bonds 1.75 and 2.20 Å, respectively) as well as with the three remaining water molecules and the Mg cation. The initially bridging anhydride oxygen O_s (ADP) interacts more strongly with the amine group of Asp157 after hydrolysis, and the H-bond shortens from 1.87 to 1.70 Å. The His161 side chain shows no catalytic activity during the course of the reaction despite its H-bond with WAT2 ($N_\delta-H$ distance 1.94−2.20 Å) that initially binds to WAT1. The Mg^{2+} coordination changes little on hydrolysis, but the initial O_β and O_γ contacts are shorter (2.05 and 2.03 Å, respectively). The separation between P_β and P_γ (4.49 Å) causes a slight tilting of the octahedral hydration shell of Mg^{2+} that is transmitted to the stabilizing side chains Asp11, Asp154, and Lys18.

C. Reactions with Two Reaction Coordinates. Information about plausible reaction paths was found by introducing two reaction coordinates that describe the nucleophilic attack of the catalytic water as the terminal phosphate is stretched apart (eq 2) or as WAT1 deprotonates (eq 3). Three reaction paths using combinations of these constraints are summarized in Figure 3 together with the corresponding transition states.[30] The order of events is changed between reaction 2 (dissociative) and reaction 3 (associative), since the deprotonation step of lytic water either follows or precedes the nucleophilic attack, and in the last reaction (reaction 4) they occur simultaneously.

The energies, values of constraint, and distances for the second reaction path are shown in Figure 4. This reaction is "dissociative", since it involves the breaking of the $P_\gamma-O_s$ bond and formation of the metastable PO_3^-, after which deprotonation occurs. The lone pair of WAT1 points initially toward the terminal phosphate, but this soon changes as the water rotates to form a hydrogen bond with a phosphoryl oxygen. A local minimum of 1.0 kcal/mol ($P_\gamma-O_w$ distance 3.28 Å) corresponds to the second WAT1 orientation reported for the reactants ($P_\gamma-O_w$ distance 3.61 Å). The distances shown in Figure 4c indicate that WAT1 approaches the phosphate rapidly during the first stage of the reaction. At a separation of 2.6 Å, the $P_\gamma-O_s$ bond starts to stretch, and it breaks within a few steps. The first transition state (TS2a, Figures 3 and 5) is observed in the crossing of $P_\gamma-O_s$ and $P_\gamma-O_w$ distances at 2.4 Å with an energy barrier of 20.4 kcal/mol. The geometry of TS2a in Figure 5 shows a planar PO_3^- unit facing O_s and O_w from opposite sides ($O_s-P_\gamma-O_w$ angle 170.5°), and it resembles a pentacoordinated transition state often discussed in the context of associative

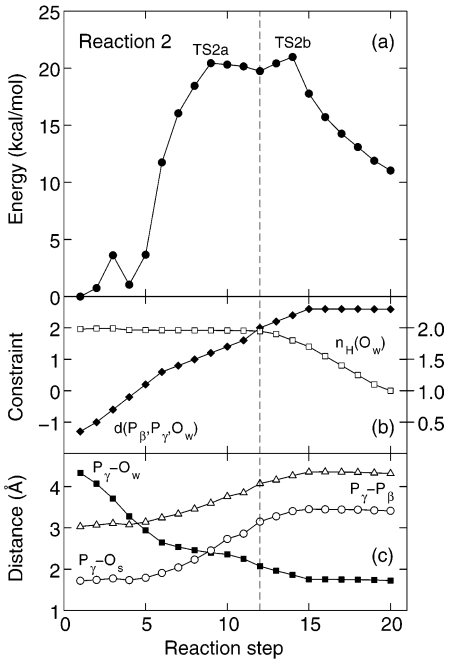

Figure 4. Dissociative reaction (reaction 2) with two reaction constraints: (a) energetics, (b) values of constraints, and (c) distances. The reaction maxima (transition states) are labeled as discussed in the text. The vertical dashed line marks the point where the second reaction coordinate ($n_H(O_w)$) becomes active.

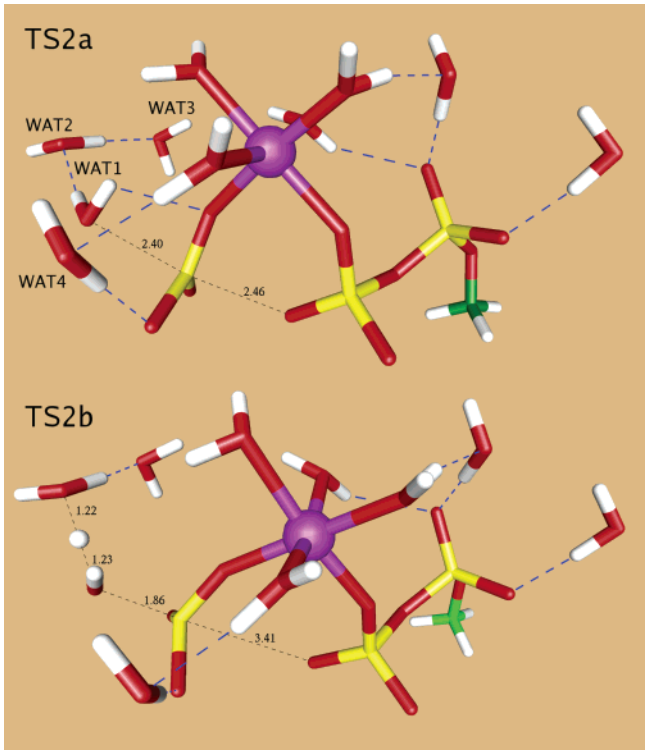

Figure 5. Local geometries of transition states TS2a and TS2b. The values for $P_\gamma-O_w$ and $P_\gamma-O_s$ distances are shown as well as the H-bond between WAT1 and WAT2 (TS2b). The dashed blue lines represent H-bonds.

reaction mechanisms.[4,31,32] The corresponding electron localization function (ELF, ref 33) (Figure 6a) shows narrow necks of blue (value 0) on both sides of the metaphosphate indicating a noncovalent interaction. The WAT1 dipole moment (3.2 D) suggests that the deprotonation activity is not higher than at the beginning.

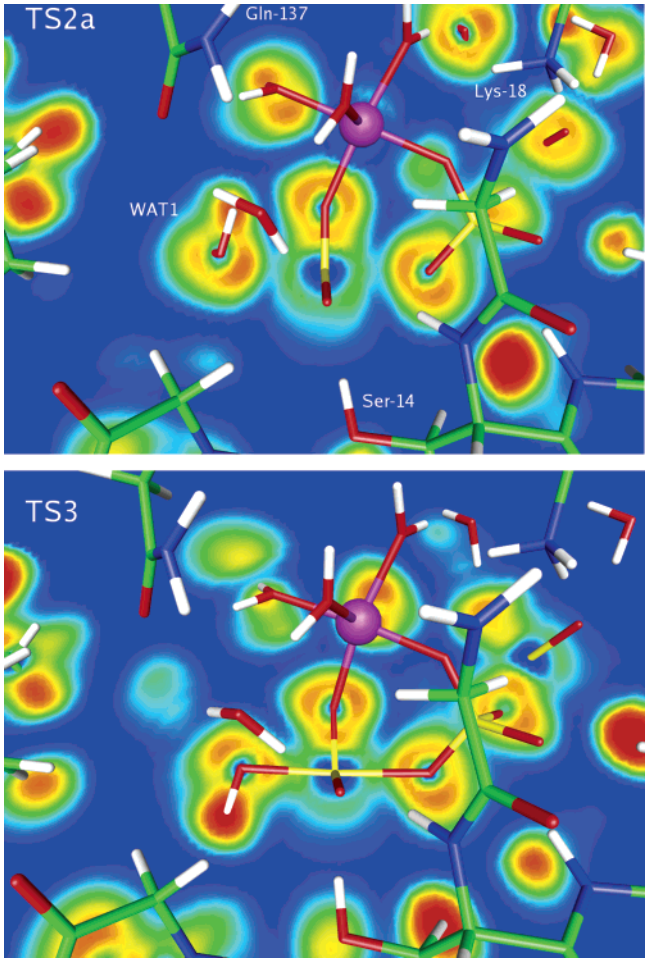

Figure 6. Electron localization function of (a) TS2a and (b) TS3. The figure is obtained by projecting ELF onto a plane containing O_w, P_γ, Mg-coordinating O_γ, and O_s. Color key: red, high localization (1.0); green, electron-gas-like localization (0.5); blue, low localization (0.0).

The first maximum is followed by a flat plateau as the phosphate cleaves, and there is a second maximum (21.0 kcal/mol, TS2b, $P_\gamma-O_w$ distance 1.86 Å) after deprotonation begins (vertical dashed line). The corresponding geometry (Figure 5) shows that the proton is in the center of WAT1 and WAT2 (O−H distances 1.22 Å) and that there is no H-bond between WAT1 and the separated γ-phosphate. Further reduction of the WAT1 protonation number completes the process as the proton diffuses via WAT2 and WAT3 to the carboxylate group (Asp154). The end products HPO_4^{2-} and ADP^{3-} are coupled by Mg^{2+} ($P_\beta-P_\gamma$ distance 4.31 Å), and they have 11.0 kcal/mol higher total energy than the reactants. The H-bond with Ser14 (1.65 Å) remains, and only one link with the protein backbone (Gly158) is broken. The His161 side group appears to be inactive and helps to stabilize the transition states. Gln137 interacts weakly with WAT1 and plays no significant role.

The first step of the third reaction path is complete deprotonation of WAT1, followed by nucleophilic attack of the OH^- ion formed. The energetics, values of constraints, and distances of this associative reaction are shown in Figure 7. Deprotonation has little effect on the interatomic distances (Figure 7c), but there are changes in the His161 side chain orientation that stabilize the H_3O^+ ion formed (WAT2) next to the catalytic OH^-, and the corresponding H-bond ($N_\delta-H$) shortens to 1.73 Å. The energy required for hydroxyl ion formation is approximately 18−20 kcal/mol, which agrees well with the theoretical value of 17.5 kcal/mol for an aqueous environment.[14]

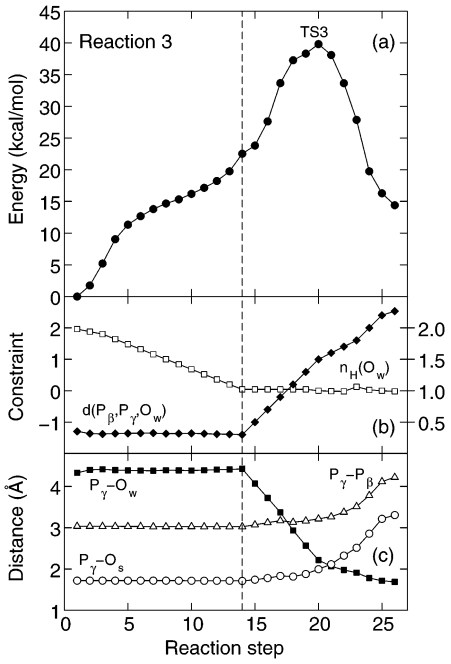

Figure 7. Associative reaction (reaction 3) with two reaction coordinates: (a) energetics, (b) values of constraints, and (c) distances. The reaction maximum (transition state) is labeled as discussed in the text. The vertical dashed line marks the point where the second reaction coordinate ($d(P_\beta,P_\gamma,O_w)$) becomes active.

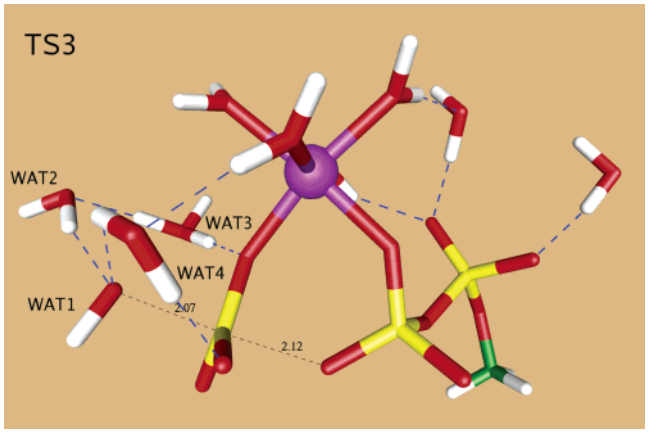

Figure 8. Local geometry of transition state TS3. The values for $P_\gamma-O_w$ and $P_\gamma-O_s$ distances are shown, and the dashed blue lines represent H-bonds.

Further reduction of the protonation number of WAT1 (H-bond elongation) results in an additional proton transfer from WAT2 to WAT3 and an increase in total energy (dashed line). The nucleophilic attack follows rapidly on implementing the second coordinate, but the energy barrier is 39.8 kcal/mol. The corresponding pentacoordinated transition state (TS3, Figure 8) is similar to TS2a, but the $P_\gamma-O_w$ and $P_\gamma-O_s$ distances are 0.3 Å shorter. In contrast to TS2a, the ELF plot (Figure 6b) shows an electron-gas-like localization (green) around PO_3^-, indicating chemical bonding with O_s and O_w. After the reaction intermediate is passed, the improper dihedral angle (defined through the nonbridging oxygens and P_γ) changes its sign according to the Walden inversion mechanism, and the $P_\gamma-O_s$ bond breaks rapidly. The metastable hydronium ion (WAT3) donates the extra proton to O_γ during the last step, and the end products are $H_2PO_4^-$ and ADP^{3-} ($P_\beta-P_\gamma$ distance 4.22 Å) corresponding to a total energy of 14.4 kcal/mol.

In contrast to His161, the orientation of the Gln137 side chain changes little, and the initial H-bond with the catalytic water

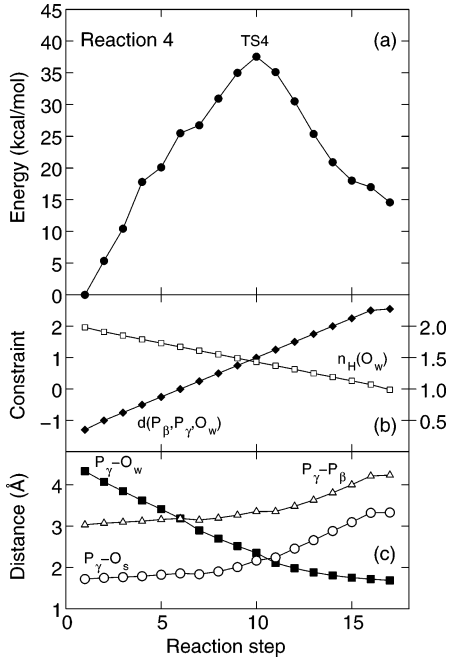

Figure 9. Reaction 4: (a) energetics, (b) values of constraints, and (c) distances.

breaks during the nucleophilic attack so that the separated phosphate is not coordinated by Gln137. The H-bond with Ser14 remains, as do the links with the backbone amine groups (Gly158 elongated). The Mg coordination changes; O_γ becomes protonated, and the Mg−O_γ distance increases to 2.31 Å.

The shortest path in Figure 3 is the fourth reaction, where two reaction coordinates are changed simultaneously. The corresponding energies, values of constraints, and distances are shown in Figure 9. The energy rises steadily to a maximum of 37.6 kcal/mol, followed by a similar decrease. WAT1 approaches first the phosphate ($P_\gamma-O_w$), and the $P_\gamma-O_s$ bond elongation starts shortly before the energy maximum. The corresponding transition state resembles closely TS3 (Figure 8) with $P_\gamma-O_s$ and $P_\gamma-O_w$ distances of 2.2 Å, but the metastable H_3O^+ is in a different location (WAT2). The end products, their coordinations, and the corresponding total energy are as in the previous reaction, and the close relationship between the two reaction paths suggests that reaction 4 could also be described as associative. In contrast to reaction 3, His161 is not more active in stabilizing H_3O^+, and the corresponding H-bond remains between 1.9 and 2.0 Å throughout.

D. Optimized Active Site: End Products. The above reactions show that the protonation and orientation of the separated phosphate vary. The most favorable energy (5.7 kcal/mol) is found for the first reaction, where $H_2PO_4^-$ is protonated at an oxygen that is not linked to Mg^{2+}. In seeking an even lower energy, we changed this configuration slightly by rotating the phosphate to make an H-bond with the initial anhydrate oxygen (O_s) in ADP^{3-}. The resulting geometry (Figure 10, ref 34) has an energy 2.1 kcal/mol below the starting value (first optimized structure). The H-bond acceptor−donor distance between O_β and O_γ is 2.48 Å ($O_\beta-H_\gamma$ distance 1.42 Å) and provides a direct connection between the two phosphates. The additional link results in a $P_\beta-P_\gamma$ distance of 4.17 Å, which is the shortest obtained for the optimized end products. The interaction with Mg^{2+} remains strong, and the corresponding Mg−O distances are 2.08 and 2.03 Å for O_β and O_γ, respectively.

The orientations of the side chains change little. The Lys18 finger and carboxylate groups of Asp11 and Asp154 are almost

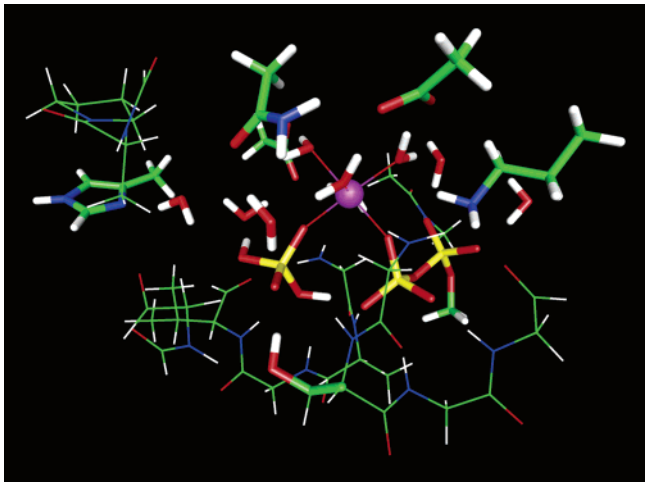

Figure 10. Optimized end products. The perspective is similar to Figure 1a. Notice that $H_2PO_4^-$ in the middle is attached to the other phosphate via an H-bond and an O−Mg−O bridge.

unchanged as the hydration shell of Mg^{2+} tilts, but deviations are seen in Gln137 and His161, which move by up to 0.8 Å due to the changes in the water cavity. His161 connects WAT2 (H-bond 1.90 Å), but Gln137 has lost contact with WAT1 during hydrolysis, and its carboxamide group forms a cyclic H-bond configuration with WAT4. The formation of two hydroxyl groups in $H_2PO_4^-$ has weakened hydrogen bonding with the protein backbone, and the contacts with Ser14, Gly158, and Val159 have increased to 2.2−2.4 Å. The H-bond with the Ser14 side chain (1.65 Å) remains the strongest link with the protein.

We have obtained additional information about possible conformational changes of the ATP−actin systems by using classical molecular mechanics. The situations before (ATP−actin) and after hydrolysis (ADP·P_i−actin, P_i refers to $H_2PO_4^-$) as well as after phosphate migration (ADP−actin) were modeled separately for 8−10 ns, and the stabilizing gelsolin segment of the initial crystal structure was removed. A snapshot of the ADP·P_i−actin system after 5 ns of molecular dynamics compared with the initial crystal structure of ATP−actin is shown in Figure 11. Structural changes are small, especially in the vicinity of the nucleotide binding cleft, and the average root-mean-square deviation (RMSD) value for backbone α-carbons is 0.66 Å. As in the experimental X-ray measurements, the largest deviation is observed in the DNase I binding loop in subdomain 2, whose conformation may depend on the nucleotide bound. However, our simulations for ATP, ADP·P_i, and ADP show few differences. Monitoring the RMSD reveals that ATP− and ADP·P_i−actin are properly thermalized, but this is not true for ADP−actin, where the RMSD first increases and then decreases slightly within 10 ns of simulation. Within our limited time scale, the absence of phosphate appears to yield a larger deviation from the initial crystal structure. It is clear that studies of real conformational changes will require simulations an order of magnitude longer.

The structure and end products of the active site of ADP·P_i−actin are very similar to the DF-optimized structure discussed above. Hydrolysis alone does not result in an immediate conformational change at the protein center, and the ionic Mg−O bonds are crucial because they keep ADP^{3-} and $H_2PO_4^-$ together. The simulation trajectory also shows no large changes in the cation hydration shell. Similarly, the H-bonds involving the two phosphates (average value 1.63 Å) and O_γ and Ser14 (1.71 Å) fix the orientation of $H_2PO_4^-$. The resulting average $P_\beta-P_\gamma$ distance (4.16 Å) is very close to the DF-optimized geometry (4.17 Å).

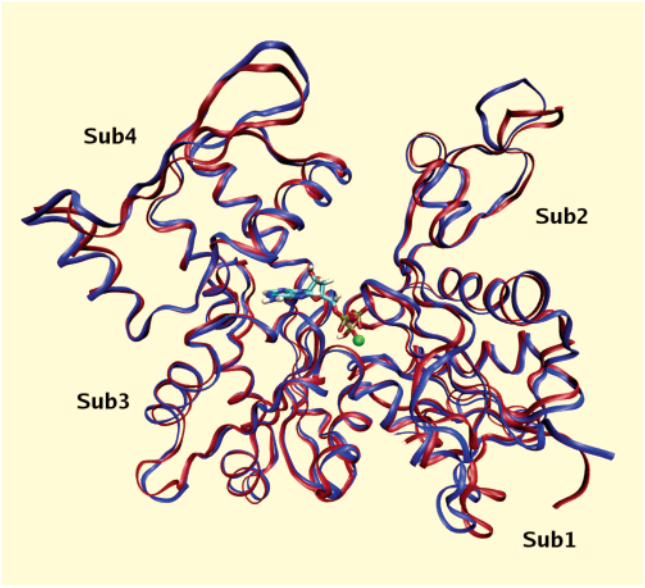

Figure 11. Snapshot of ADP·P_i−actin after 5 ns of molecular dynamics (blue ribbons) compared to the initial crystal structure of ATP−actin (red ribbons). The actin subdomains are labeled according to the standard notation. ADP^{3-} and $H_2PO_4^-$ are shown in the licorice format, and the Mg cation is represented by a green sphere (simulation).

Comparison of ATP− and ADP·P_i−actin shows that the catalytically important Gln137 and His161 side chains are accessible to the separated phosphate. The Gln137 side chain in the ATP state does not connect to the terminal phosphate at any time, while the hydroxyl group of $H_2PO_4^-$ binds occasionally to the carbonyl oxygen of Gln137. Similarly, His161 does not reach the terminal phosphate before hydrolysis, but it forms frequent H-bonds with the separated phosphate via its protonated imidazole nitrogen (N_ϵ). Gln137 and His161 are important for hydrolysis and the final phosphate cleaving process, where $H_2PO_4^-$ passes through the active site "back door" to yield ADP−actin.[35] Trajectories of γ-phosphate in contact with H_2O show diminished mobility, and in only one case (WAT1, ATP−actin) did a water molecule leave the nucleotide binding cleft while being replaced by another.

IV. Discussion and Concluding Remarks

ATP hydrolysis at the active site of actin has been studied using a DF method. The active site is approximated by the reactive triphosphate tail of ATP complexed with Mg^{2+}, the surrounding water molecules, and the nearest actin residues. This model system includes the reactive cavity of four water molecules (WAT1−WAT4) and γ-phosphate, all triphosphate coordinating residues, and a full hydration shell of Mg with stabilizing aspartate side chains. The large system size enables us to study important aspects in the ATP hydrolysis (reaction paths, catalytically important residues, proton wires, role of divalent cations, and coordination of end products), and it includes a significant portion of the electrostatic field imposed by the whole protein. The calculations use an extended plane wave basis and are very demanding in terms of CPU time and memory.

Four reaction paths have been modeled by constraining certain coordinates, and the first gives the simplest picture of dissociative path as the bridging $P_\gamma-O_s$ bond is stretched. A barrier of 28.8 kcal/mol is obtained at 2.8 Å, after which the metaphosphate formed is approached by WAT1, which is in contact with PO_3^- via its lone pair orbital. A further increase in the $P_\gamma-O_s$ distance results in spontaneous deprotonation of WAT1 that transfers a proton to the phosphate via a proton wire (WAT2 and WAT3). This path supports the suggestion that WAT1 is the catalytic water, because its location enables an in-line nucleophilic attack on the terminal phosphorus. However, the local dipole moment of WAT1 (3.1 D) in the initial configuration differs little from that of bulk water.

The other reactions employ two coordinates that control (a) the nucleophilic attack of the catalytic water as the β- and γ-phosphates are separated and (b) the protonation number of WAT1. The three paths display different orders of events and can be characterized as dissociative (reaction 2) or associative (reactions 3 and 4). The lowest-energy barrier is for reaction 2, where the terminal phosphate is cleaved (20.4 kcal/mol, TS2a), and the deprotonation of WAT1 follows (21.0 kcal/mol, TS2b). These two events compensate for each other energetically and lead to the flat plateau in total energy between TS2a and TS2b. In the structure TS2a the dipole moment of WAT1 is relatively small (3.2 D) and the interaction with the metaphosphate is noncovalent ($P_\gamma-O_w$ distance 2.4 Å). The reaction is completed when a proton is transferred to a carboxylate group of Asp154, resulting in a cleaved HPO_4^{2-}.

In the associative reaction 3, deprotonation of WAT1 results in a reactive OH^- ion, which then makes a nucleophilic attack on P_γ. The barrier obtained (39.8 kcal/mol, TS3) is significantly higher than those for the previous reactions, but it agrees well with our study of ATP hydrolysis in water (39.1 kcal/mol)[4] and the results of Okimoto (42.0 kcal/mol) for ATP hydrolysis in an isolated active site of myosin.[31] The corresponding transition state contains a pentacoordinated phosphorus with $P_\gamma-O_s$ and $P_\gamma-O_w$ distances of 2.1 Å, and the ELF shows electron-gas-like localization of electron density that indicates chemical bonding. Reaction 4 displays features that are very similar to those of reaction 3, although nucleophilic attack is concurrent with the deprotonation of WAT1. The barrier is 37.6 kcal/mol.

Associative reactions are energetically unfavorable, perhaps because deprotonation of WAT1 costs a significant amount of work. To accommodate a proton transfer, the protein has to modify the pK_a of WAT1 via a conformational change. Indications of environment-assisted deprotonation are observed in reaction 3 as the H-bond between the imidazole group of His161 (base) and WAT2 shortens during H_3O^+ formation. It has been proposed that in the reactive conformation His161 should bind to WAT1, as in the X-ray measurement for Li^+−ATP actin, and this is consistent with the large fluctuations in the His161 side chain location found in our molecular mechanics simulations of ATP−actin. However, the mobility of Gln137 is not enhanced, and it is an unlikely base for WAT1, which prefers to transfer a proton to WAT2 as $n_H(O_w)$ is decreased. The probable role of Gln137 in ATP hydrolysis is to place WAT1 in a preferable position and orientation.

The four reactions lead to different protonation and coordination of end products. The most energetically favorable situation is achieved when a nonbridging O_γ (not linked to Mg^{2+}) is protonated resulting in $H_2PO_4^-$ and ADP^{3-}, which are coupled by a H-bond. Classical simulations (8 ns) of ADP·P_i−actin confirm the importance of the phosphate orientation where the initial $Mg-O_\gamma$ linkage is preserved. The total energy (−2.1 kcal/mol) is slightly below the starting level but less than typical values for ATP hydrolysis in aqueous solution (−5 to −10 kcal/mol).[15,36,37] We suspect that the complete cleavage of $H_2PO_4^-$ can release additional energy. Comparison of ATP− and ADP·P_i−actin structures reveals few differences (especially at the active site), and a phosphate migration appears crucial for a conformational change (ADP−actin). Simulations for ADP·P_i−

actin show that the catalytically important residues Gln137 and His161 bind occasionally to the inorganic phosphate, in agreement with the results of Wriggers and Schulten.[35] The rate-limiting step for P_i release is probably the breaking of the strong $O_\beta-Mg-O_\gamma$ bridge where one water replaces O_γ and completes the octahedral hydration shell of Mg^{2+}. Further simulations of the phosphate release process and nucleotide binding in actin are in progress.

Acknowledgment. The DF calculations were performed on the IBM p690 supercomputer (JUMP) in the Forschungszentrum Jülich with grants of computer time from the FZJ and the John von Neumann Institute for Computing. The classical force field simulations were performed on Xeon and Athlon processors supported in part by the Bundesministerium für Bildung und Wissenschaft, Bonn, within the MaTech-Kompetenzzentrum "Werkstoffmodellierung" (03N6015). We thank F. Gervasio, D. Branduardi (ETH Zürich), and M. Ceccarelli (University of Cagliari) for support and helpful discussions.

References and Notes

(1) Boyer, P. D. *Nobel Lectures, Chemistry 1996−2000*; Grenthe, I., Ed.; World Scientific Publishing: Singapore, 2003; p 120.
(2) De La Cruz, E. M.; Pollard, T. D. *Biochemistry* **1995**, *34*, 5452.
(3) Melki, R.; Fievez, S.; Carlier, M.-F. *Biochemistry* **1996**, *35*, 12038.
(4) Akola J.; Jones R. O. *J. Phys. Chem. B* **2003**, *107*, 11774.
(5) Vorobiev, S.; Strokopytov, B.; Drubin, D. G.; Frieden, C.; Ono, S.; Condeelis, J.; Rubenstein, P. A.; Almo, S. C. *Proc. Natl. Acad. Sci. U.S.A.* **2003**, *100*, 5760.
(6) Mildvan, A. S. *Proteins* **1997**, *29*, 401.
(7) Hutter, J. et al. *CPMD Program*, version 3.7; Max-Planck-Institut für Festkörperforschung and IBM Research: 1990−2003.
(8) Akola, J.; Jones, R. O. *J. Phys. Chem. B* **2006**, *110*, 8110.
(9) Perdew, J. P.; Burke, K.; Ernzerhof, M. *Phys. Rev. Lett.* **1996**, *77*, 3865.
(10) Troullier, N.; Martins, J. L. *Phys. Rev. B* **1991**, *43*, 1993.
(11) Hockney, R. W. *Methods Comput. Phys.* **1970**, *9*, 136.
(12) Graceffa, P.; Dominguez, R. *J. Biol. Chem.* **2003**, *278*, 34172.
(13) Nyman, T.; Schüler, H.; Korenbaum, E.; Schutt, C. E.; Karlsson, R.; Lindberg, U. *J. Mol. Biol.* **2002**, *317*, 577.
(14) Sprik, M. *Chem. Phys.* **2000**, *258*, 139.
(15) George, P.; Witonsky, R. J.; Trachtman, M.; Wu, C.; Dorwart, W.; Richman, L.; Richman, W.; Shurayh, F.; Lentz, B. *Biochim. Biophys. Acta* **1970**, *223*, 1.
(16) See, for example, Carloni, P.; Röthlisberger, U.; Parrinello, M. *Acc. Chem. Res.* **2002**, *35*, 455.
(17) Procacci, P.; Darden, T. A.; Paci, E.; Marcchi, M. *J. Comput. Chem.* **1997**, *18*, 1848. The nucleotide−actin systems (5840 atoms) are solvated by 10 950 water molecules in an orthorhombic box of $61.2 \times 79.5 \times 79.5$ $Å^3$.
(18) Essmann, U.; Perera, L.; Berkowitz, M. L.; Darden, T.; Lee, H.; Pedersen, L. G. *J.Chem. Phys.* **1995**, *101*, 8577.
(19) Cornell, W. D.; Cieplak, P.; Bayly, C. I.; Gould, I. R.; Merz, K. M.; Ferguson, D. M.; Spellmeyer, D. C.; Fox, T.; Caldwell J. W.; Kollman, P. A. *J. Am. Chem. Soc.* **1995**, *117*, 5179.
(20) Meagher, K. L.; Redman, L. T.; Carlson, H. A. *J. Comput. Chem.* **2003**, *24*, 1016.
(21) Schüler, H.; Korenbaum, E.; Schutt, C. E.; Lindberg, U.; Karlsson, R. *Eur. J. Biochem.* **1999**, *265*, 210.
(22) Belmont, L. D.; Orlova, A.; Drubin, D. G.; Egelman, E. H. *Proc. Natl. Acad. Sci. U.S.A.* **1999**, *96*, 29.
(23) Schüler, H.; Nyåkern, M.; Schutt, C. E.; Lindberg, U.; Karlsson, R. *Eur. J. Biochem.* **2000**, *267*, 4054.
(24) Berghold, G.; Mundy, C. J.; Romero, A. H.; Hutter, J.; Parrinello, M. *Phys. Rev. B* **2000**, *61*, 10040.
(25) Silvestrelli, P. L.; Parrinello, M. *Phys. Rev. Lett.* **1999**, *82*, 3308.
(26) The effective charge is obtained by integrating over the electron density in the Wigner−Seitz cell of the cation.
(27) Minehardt, T. J.; Marzari, N.; Cooke, R.; Pate, E.; Kollman P. A.; Car, R. *Biophys. J.* **2002**, *82*, 660.
(28) A three-dimensional rotatable image in xyz-format is available (Reactants.xyz).
(29) Cini, R.; Burla, M. C.; Nunzi, A.; Polidori, P. G.; Zanazzi, P. *J. Chem. Soc., Dalton Trans.* **1984**, 2467.
(30) Three-dimensional rotatable images of Reactions 2 and 3 are available in xyz-format (Reaction2.xyz, Reaction3.xyz).
(31) Okimoto, N.; Yamanaka, K.; Ueno, J.; Hata, M.; Hoshino, T.; Tsuda, M. *Biophys. J.* **2001**, *81*, 2786.
(32) Boero, M.; Terakura, K.; Tateno, M. *J. Am. Chem. Soc.* **2002**, *124*, 8949.
(33) See, for example, Savin, A.; Nesper, R.; Wengert, S.; Fässler, T. F. *Angew. Chem., Int. Ed. Engl.* **1997**, *36*, 1808.
(34) A three-dimensional rotatable image in xyz-format is available (End-products.xyz).
(35) (a) Wriggers, W.; Schulten, K. *Biophys. J.* **1997**, *73*, 624. (b) Wriggers, W.; Schulten, K. *Proteins: Struct., Funct., Genet.* **1999**, *35*, 262.
(36) Romero, P. J.; de Meis, L. *J. Biol. Chem.* **1989**, *264*, 7869.
(37) de Meis, L. *Biochim. Biophys. Acta* **1989**, *973*, 333.